conclude that there is evidence, but not proof, that the mid-latitude sources are associated with the Gould belt.

The third EGRET catalogue will be the best data set in high-energy γ-ray astronomy for years to come. (This is because the spark chamber gas in the EGRET instrument is almost completely used up.) With these data we have evidence that the unidentified high-energy γ-ray sources are made up of two separate populations. There must be distinctly different types of objects that make up the two groups. The bright sources are in the Galactic plane and therefore at large (kiloparsec) distances, whereas the weak sources are off the plane and presumably at the 100–400-pc distances of the Gould belt. This implies that the luminosities of the mid-latitude sources are much lower than those of the sources in the Galactic plane. The luminosity difference is of the order of a factor of 3 (for the brightest difference) times 25 (for the square of the distance difference): a total of a factor of ~75.

What kinds of sources are likely to be the counterparts of the mid-latitude objects if they are truly in the Gould belt? Objects that are known to be, or thought likely to be, high-energy γ-ray emitters include molecular clouds[18] (cosmic rays interacting with the enhanced gas concentrations in the clouds to produce γ-ray enhancements in the sky), supernova remnants[19–22] (cosmic rays accelerated in the supernova explosion interacting with gas in the vicinity to produce γ rays), massive stars[21,22] (γ rays produced in the outflowing winds from the stars) and pulsars[10,23,24] (γ rays produced in the particle acceleration regions of the pulsar magnetospheres). Because the Gould belt has an enhanced concentration of massive stars and molecular gas concentrations, we speculate that the γ rays from the mid-latitude sources are produced in these two types of objects. This hypothesis will be tested in 2005 with the launch of the GLAST mission[25]. Its high sensitivity and improved angular resolution relative to EGRET will allow unique counterparts to be found for the individual unidentified sources. □

Received 8 October 1999; accepted 5 January 2000.

1. Swannenburg, B. N. *et al.* Second COS B catalog of high-energy gamma-ray sources. *Astrophys. J.* **243,** L69–L73 (1981).
2. Hartman, R. C. *et al.* The Third EGRET catalog of high-energy gamma-ray sources. *Astrophys. J. Supp.* **123,** 79–202 (1999).
3. Gould, B. A. *Brillantez y posicion de las estrellas fijas, hasta la septima magnitud, comprendidas dentro de cien grados del polo austral: con atlas, Uranometria Argentina* (ed. Corni, P. E.) 354 (Buenos Aires, 1879).
4. Guillout, P. *et al.* Discovery of a late-type stellar population associated with the Gould Belt. *Astron. Astrophys.* **337,** 113–124 (1998).
5. Grenier, I. A. & Perrot, C. Enhanced pulsar and cosmic-ray production in the Gould Belt? *Proc. XXVI Int. Cosmic Ray Conf. Salt Lake City* **3,** 476–479 (1999).
6. Thompson, D. J. Calibration of the Energetic Gamma-Ray Experiment Telescope (EGRET) for the Compton Gamma-Ray Observatory. *Astrophys. J. Suppl.* **86,** 629–656 (1993).
7. Mattox, J. R. *et al.* The likelihood analysis of EGRET data. *Astrophys. J.* **461,** 396–407 (1996).
8. Hunter, S. D. *et al.* EGRET observations of the diffuse gamma-ray emission from the Galactic plane. *Astrophys. J.* **481,** 205–240 (1997).
9. Grenier, I. A. Spatial distribution of the unidentified EGRET sources off the Galactic plane. *Adv. Space Res.* **15,** 73–76 (1995).
10. Romani, R. W. & Yadigaroglu, I.-A. Gamma-ray pulsars: Emission zones and viewing geometries. *Astrophys. J.* **438,** 314–321 (1995).
11. Ozel, M. E. & Thompson, D. J. On the nature of unidentified 2EG sources at high latitudes. *Astrophys. J.* **463,** 105–109 (1996).
12. Lamb, R. C. & Macomb, D. J. Point sources of GeV gamma rays. *Astrophys. J.* **488,** 872–880 (1997).
13. Dixon, D. D. *et al.* Evidence for a Galactic gamma-ray halo. *New Astron.* **3,** 539–558 (1998).
14. Stothers, R. & Frogel, J. A. The local complex of 0 and B stars: I. Distribution of stars and interstellar dust. *Astron. J.* **79,** 456–471 (1974).
15. Taylor, D. K., Dickman, R. L. & Scoville, N. Z. Molecular clouds and the Gould belt. *Astrophys. J.* **315,** 104–121 (1987).
16. Lindblad, P. O., Grupe, K., Sandqvist, Aa. & Schuber, J. On the kinematics of a local component of the interstellar hydrogen gas possibly related to Gould's Belt. *Astron. Astrophys.* **24,** L309–L312 (1973).
17. Olano, C. A. On a model of local gas related to Gould's belt. *Astron. Astrophys.* **112,** 195–208 (1982).
18. Houston, B. P. & Wolfendale, A. W. Galactic gamma radiation- The contribution from discrete sources. *Astron. Astrophys.* **126,** 22–30 (1983).
19. Sturner, S. J. & Dermer, C. D. Association of unidentified, low latitude EGRET sources with supernova remnants. *Astron. Astrophys.* **293,** L17–L20 (1995).
20. Esposito, J. A. *et al.* EGRET observations of radio-bright supernova remnants. *Astrophys. J.* **461,** 820–827 (1996).
21. Romero, G. E., Benaglia, P. & Torres, D. F. Unidentified 3EG gamma-ray sources at low Galactic latitudes. *Astron. Astrophys.* **348,** 868–876 (1999).
22. Montmerle, T. On gamma-ray sources, supernova remnants, OB associations, and the origin of cosmic rays. *Astrophys. J.* **231,** 95–110 (1979).
23. Thompson, D. J. *et al.* EGRET high-energy gamma-ray pulsar studies. 1: Young spin-powered pulsars. *Astrophys. J.* **436,** 229–238 (1994).
24. Kaaret, P. & Cottam, J. Do the unidentified Galactic EGRET sources lie in star-forming regions? *Astrophys. J.* **462,** L35–L38 (1996).
25. Gehrels, N. & Michelson, P. GLAST: the next-generation high energy gamma-ray astronomy mission. *Astroparticle Phys.* **11,** 277–282 (1999).

Acknowledgements

We thank I. Grenier and S. Hunter for discussions.

Correspondence and requests for materials should be addressed to N. G. (e-mail: gehrels@gsfc.nasa.gov).

Trapping an atom with single photons

P. W. H. Pinkse, T. Fischer, P. Maunz & G. Rempe

Max-Planck-Institut für Quantenoptik, Hans-Kopfermann-Strasse 1, 85748 Garching, Germany

The creation of a photon–atom bound state was first envisaged for the case of an atom in a long-lived excited state inside a high-quality microwave cavity[1,2]. In practice, however, light forces in the microwave domain are insufficient to support an atom against gravity. Although optical photons can provide forces of the required magnitude, atomic decay rates and cavity losses are larger too, and so the atom–cavity system must be continually excited by an external laser[3,4]. Such an approach also permits continuous observation of the atom's position, by monitoring the light transmitted through the cavity[5–9]. The dual role of photons in this system distinguishes it from other single-atom experiments such as those using magneto-optical traps[10–12], ion traps[13,14] or a far-off-resonance optical trap[15]. Here we report high-finesse optical cavity experiments in which the change in transmission induced by a single slow atom approaching the cavity triggers an external feedback switch which traps the atom in a light field containing about one photon on average. The oscillatory motion of the trapped atom induces oscillations in the transmitted light intensity; we attribute periodic structure in intensity-correlation-function data to 'long-distance' flights of the atom between different anti-nodes of the standing-wave in the cavity. The system should facilitate investigations of the dynamics of single quantum objects and may find future applications in quantum information processing.

The interaction of a single two-level atom with a single mode of

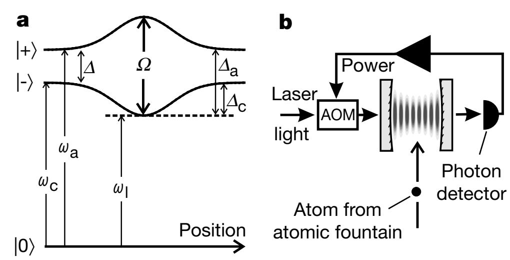

Figure 1 Atom–cavity system. **a**, Ground state and the first excited states of the atom–cavity system as a function of the atom's position in a gaussian mode. The dressed states $|-\rangle$ and $|+\rangle$ are linear combinations of the uncoupled states, with coefficients that depend on Ω. The arrows indicate the frequencies of the atom (ω_a), the cavity (ω_c) and the laser (ω_l). The cavity transmission is high if ω_l is close to one of the dressed states. **b**, Experimental set-up. Atoms are launched by an atomic fountain towards the high-finesse cavity. An acousto-optic modulator (AOM) triggered by the presence of an atom in the cavity increases the light intensity.

the electromagnetic field is well described by the Jaynes–Cummings model[16]. The dipole interaction couples the atom and the cavity field, leading to new (dressed) energy eigenstates that are combinations of the bare atom and cavity states. The frequency difference, $\Omega = \sqrt{\Delta^2 + 4g_0^2\psi(\mathbf{r})^2}$, between the two dressed states containing one quantum of excitation is determined by the atom–cavity detuning, $\Delta = \omega_c - \omega_a$, the cavity-field mode function, $\psi(\mathbf{r})$, and the atom–field coupling constant at an antinode, g_0, where $\psi(\mathbf{r}) = 1$ by definition. Figure 1a displays the dressed energy levels as a function of position for a gaussian mode profile. The pump laser induces transitions between these states with a rate given by the laser intensity, its frequency, ω_l, and the atom's position, $\mathbf{r}$. The excitation probability determines the cavity transmission and, hence, allows us to observe the atomic motion. Indeed, the transmitted light is a direct measure for the strength of the atom–field coupling. The dipole force on the atom, created by the exchange of a photon between the atom and the cavity field, is given by the negative gradient of the energy of the dressed state, $|+\rangle$ or $|-\rangle$, multiplied by the excitation probability. The energy minimum of state $|-\rangle$, in particular, facilitates three-dimensional atom trapping in the centre of the cavity. In addition to this conservative force, a velocity-dependent force and momentum diffusion induced by spontaneous emission and dipole fluctuations are important. For a weak pump laser, analytical expressions exist for these forces[17,18], all confirmed in a recent experiment where the oscillatory motion of atoms channelling through the nodes or antinodes of a standing-wave cavity field containing less than one photon on average was analysed in detail[4]. For larger excitation, more states than just the ground state and the first two excited states must be taken into account. In that case no analytical solutions for the forces are available and the system's master equation must be solved numerically. Experimentally, cooling and three-dimensional mechanical binding of atoms has not been observed in this system, so far.

We emphasize that the quantum character of the cavity field, that is, its granular nature with associated fluctuations in the number of photons, does not affect the steady-state dipole force and velocity-dependent force. It does, however, increase the momentum diffusion compared to that in a coherent light field[18]. The reason is the back action of the atom on the cavity field, which is not found, for example, in a far-off-resonance dipole trap[15].

The experimental set-up is shown in Fig. 1b. A pulsed atomic fountain launches laser-cooled rubidium (^{85}Rb) atoms towards a high-finesse cavity. The flux of atoms is kept so low that at most one atom resides in the cavity at any time. The atoms are optically pumped into the $F = 3$, $m_F = 3$ Zeeman sublevel of the $5^2S_{1/2}$ ground state and the spin orientation is maintained by a small magnetic bias field. The cavity has a finesse of $\sim 4.3 \times 10^5$ and a length of 116 μm, which is actively stabilized, with the exception of the measuring interval of a few milliseconds, during which an atom can be present in the cavity. The cavity field is pumped by a circularly polarized TEM_{00}-mode laser beam, near resonant with the $5^2S_{1/2}$, $F = 3 \leftrightarrow 5^2P_{3/2}$, $F = 4$ transition of the atom at a wavelength of $\lambda = 780$ nm. The intensity and the frequency of this light is controlled by an acousto-optic modulator. The cavity mode function is $\psi(\mathbf{r}) = \cos(2\pi z/\lambda)\exp[-(x^2 + y^2)/w_0^2]$, with waist $w_0 = 29\,\mu$m and the z-axis horizontal. The light transmitted through the cavity is focused onto a single-photon counting detector with a quantum efficiency of 60%. An additional laser beam resonant with the $5^2S_{1/2}$, $F = 2 \leftrightarrow 5^2P_{3/2}$, $F = 3$ transition of ^{85}Rb is injected into the gap between the cavity mirrors. It re-pumps the atom from the uncoupled $5^2S_{1/2}$, $F = 2$ ground state, which would otherwise be populated owing to non-perfect circular polarization of the light in the cavity during the long observation times realized in the experiment. The atom–field coupling constant, $g_0 = 2\pi \times 16$ MHz, atomic dipole decay rate, $\gamma = 2\pi \times 3$ MHz, and cavity field decay rate, $\kappa = 2\pi \times 1.4$ MHz, determine the dimensionless parameters describing the physics of our system: the saturation photon number $\gamma^2/2g_0^2 = 1/57$ and the critical atom number $2\gamma\kappa/g_0^2 = 1/30$. The potential depth for an atom trapped at an antinode of a red-detuned single-photon field is limited to $\hbar g_0$, corresponding to a temperature of 0.8 mK.

To facilitate atom trapping, we first set the atomic fountain to inject very slow atoms ($\sim$20 cm s^{-1}) into the cavity. Figure 2a displays a transmission signal in the case where we passively observe an atom passing through the cavity. The transit time of this atom amounts to 0.12 ms, consistent with the known entrance velocity. Now we turn on our feedback switch which triggers, at time $t = 0$, when an atom is detected in the cavity, increasing the intensity of the laser light impinging on the cavity within 20 μs. This increase of the potential barrier compensates the kinetic energy of the atom. Figure 2b shows a record of the power transmitted through the cavity in a successful event. The atom that triggered the feedback switch in Fig. 2b remains in the cavity for as long as 0.4 ms. After 1.1 ms, the laser power is switched back to its original value. This allows

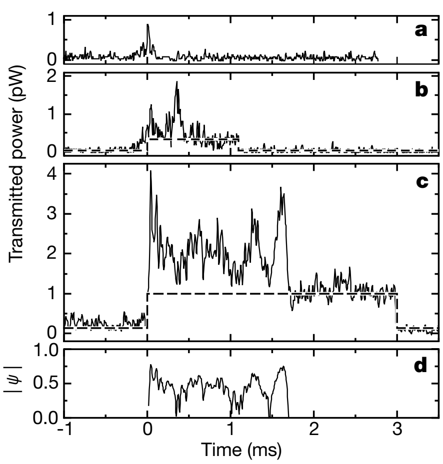

Figure 2 Experimental trajectories. **a**, Transit signal of an atom passing through the high-finesse cavity (solid lines). The detunings are $\Delta_a = \omega_l - \omega_a = -2\pi \times 40$ MHz and $\Delta_c = \omega_l - \omega_c = -2\pi \times 5$ MHz. When pumped with a power of about 150 pW at a detuning of 5 MHz and without the atom, the cavity contains one photon on average, which corresponds to a transmitted power of 0.9 pW. **b**, Same as in **a**, but with feedback. At $t = 0$, the feedback switch triggers an eight-fold increase of the pump power, as is indicated by the dashed line. As a result, the atom causing the trigger remains in the cavity for about 0.4 ms. The pump is switched back to its original value after 1.1 ms. **c**, Same as in **b**, but now with twice the light power and a measurement interval of 3 ms. The atom stays in the cavity for 1.7 ms. The detunings are $(\Delta_a, \Delta_c) = 2\pi \times (-45, -5)$ MHz. **d**, Normalized coupling $|\psi|$ of the atom as inferred from the data in **c**.

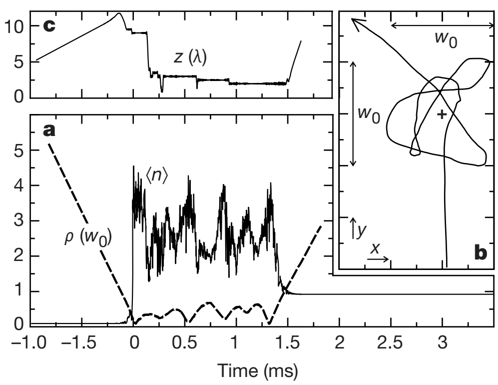

Figure 3 Atomic trajectory calculated with a quantum jump Monte Carlo method. **a,** The solid line shows the mean intracavity photon number and the dashed line indicates the radial ($\rho = \sqrt{x^2 + y^2}$) excursion of the atom. **b**, An axial view. The cross indicates the cavity axis. **c**, The axial (z) motion of the atom.

us to check the length stability of the resonator. The rare events with large resonator drifts are filtered out and discarded.

Demonstration of trapping requires direct evidence for a restoring force, indicated, for example, by an oscillatory motion of the atom. For this purpose, we must examine the transmission signal in more detail. A higher photon flux facilitates this. We therefore slightly increase the laser power in the experiments described below. Figure 2c shows an example where, for a laser intensity twice as large, the atom remains in the cavity for as long as 1.7 ms. This signal is now used to investigate the motion of this particular atom.

As mentioned in the introduction, a transit signal like that in Fig. 2c can directly be mapped onto a time-dependent atom–field coupling. The result is shown in Fig. 2d, where the normalized coupling, $|\psi|$, is plotted, providing the first information about the trajectory of this particular atom. More physical insight into the atomic motion can be obtained by comparing the experimental data with the results of a numerical simulation. Atomic trajectories are calculated using a quantum-jump Monte Carlo (QJMC) simulation[19,20]. In this simulation, the atom and the light field are treated quantum mechanically, whereas the motion of the atom is still treated classically. Gravity is neglected, because the optical forces are much larger, even in the weakly confining radial direction. A QJMC simulation is a stochastic solution of the system's master equation, in which the evolution of the quantum state describing the system is computed by combining the coherent evolution with quantum jumps that simulate the spontaneous loss of an excitation out of the system.

Figure 3 shows a result of the QJMC simulation calculated for the parameters of Fig. 2c. Plotted in Fig. 3a are the atom's distance from the cavity axis, $\rho(t)$, and the corresponding mean number of photons in the cavity, $\langle n \rangle$. In this particular simulation, the atom remains trapped for 1.4 ms. During this time interval, the atom oscillates in the radial direction with a period of about 250 μs and an amplitude of about $w_0/2$. The oscillations in the mean photon number clearly correlate with the radial excursions of the atom. From this we conclude that the oscillations observed in the experiment, characterized by the same period and similar intensity changes, are direct evidence for the radial oscillation of the atom. In particular, the transmission is large or small for an atom close to or far away from the cavity axis, respectively.

Figure 3b displays the atomic motion projected onto the xy-plane perpendicular to the cavity axis. The atom enters from below, makes a diffusive motion around the cavity axis, and leaves towards the upper left. We note that the atom's angular momentum changes because of random momentum kicks associated with spontaneous emission events. In the xy-plane, because of the cylindrical symmetry, only the distance to the cavity axis enters the atom–field coupling. It is therefore not possible to reconstruct the full three-dimensional trajectory of the atom from our experimental data.

We now study motion along the cavity axis. The strong confinement of the atom to regions of length $\lambda/2$ in the axial direction leads to a fast oscillation of the atom with a period of typically a few microseconds. These oscillations, reported in ref. 4, are not visible on the timescale of Fig. 3c. Apart from these oscillations, the atom sometimes escapes from an antinode. This is attributable to dipole fluctuations heating the atom, as mentioned in the introduction. It then hops over a few nodes, is cooled by the friction force and is finally recaptured in another antinode[17,18].

Experimental evidence for these 'long-distance' flights comes from the fourth-order intensity-correlation function of the transmitted light, $g^{(4)}(\epsilon,\tau,\epsilon)$, determined from a time-resolved record of the photon-arrival times. This record is used to calculate a second-order intensity-autocorrelation function of events defined by pairs of photons separated by only a short time interval of less than $\epsilon =$ 150 ns, discarding isolated photons. As in ref. 4, corrections were made to take into account the finite observation window. Our method of correlating photon pairs enhances intensity fluctuations because the probability of finding a photon pair scales with the square of the light intensity. A typical result from a section, 20 μs in length, of the transit signal from Fig. 2c centred at time $t = 1.51$ ms is displayed in Fig. 4a. These data are now compared with the results of our QJMC simulation, were the atomic trajectory is known. Analysing only a section where the atom moves across several antinodes, as indicated in Fig. 4c, gives the result plotted in Fig. 4b. Both the experimental curve and the simulated curve show a similar periodic modulation. If, in contrast, a section from the simulation with the atom oscillating around an antinode is analysed, hardly any periodic structure is visible. From this we conclude that the periodic modulation in Fig. 4a is direct evidence for the atom moving along the cavity axis.

Based on our detailed understanding of atomic motion, we conclude that atoms with transmission signals like those in Fig. 2b and c are actually trapped in a light field containing one or two photons on average, respectively. When we average over all events where the feedback switch triggered, we find, by fitting an exponential decay curve, an average trapping time of $\tau = 0.25 \pm 0.05$ ms. The same result is found from the QJMC simulation. The trapping time is limited by spontaneous emission kicks causing the atom to escape in the radial direction. This might be prevented by applying feedback-based cooling schemes[21]. One expects quantum aspects in the atomic motion if the atom becomes so cold that a wave description is necessary. It might even be possible to cool the atom into the quantum-mechanical ground state of the optical potential. From the continuous observation of a localized atomic wave packet by means of a quantized light field and the back action resulting from the measurement, new insights into the dynamical behaviour of an individual quantum object can be obtained. Moreover, a single particle trapped in a high-finesse cavity has applications in the rapidly growing field of quantum communication. For example, it should allow the transmission of quantum bits between distant cavities[22], to build arbitrary states of the electromagnetic field[23], or to generate a bit stream of single-mode photons[24,25]. □

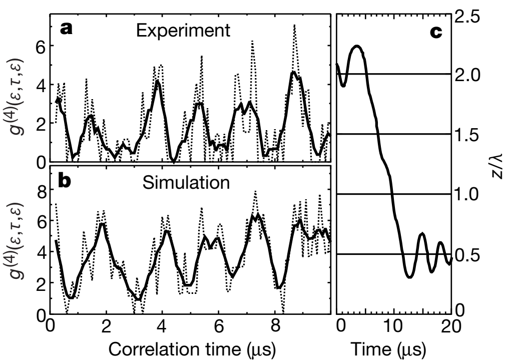

Figure 4 Short-time structure. **a**, **b**, The dashed lines are the fourth-order intensity-autocorrelation function $g^{(4)}(\epsilon,\tau,\epsilon)$. The solid lines are obtained by smoothing. **a** is taken from a section, 20 μs in length, of experimental data centred at 1.51 ms of Fig. 2c; **b** is from an equally long piece of a simulated trajectory, of which the z-coordinate is shown in **c**. The oscillations in **a** and **b** indicate a modulation of the cavity light intensity with a period of 1.8 μs and 2 μs, respectively. The oscillations in **b** are caused by the atom's motion along the z-axis, crossing an antinode (thin lines in **c**) every 2 μs.

Received 8 November 1999; accepted 28 January 2000.

1. Haroche, S., Brune, M. & Raimond, J. M. Trapping atoms by the vacuum field in a cavity. *Europhys. Lett.* **14,** 19–24 (1991).
2. Englert, B.-G., Schwinger, J., Barut, A. O. & Scully, M. O. Reflecting slow atoms from a micromaser field. *Europhys. Lett.* **14,** 25–31 (1991).
3. Hood, C. J., Chapman, M. S., Lynn, T. W. & Kimble, H. J. Real-time cavity QED with single atoms. *Phys. Rev. Lett.* **80,** 4157–4160 (1998).
4. Münstermann, P., Fischer, T., Maunz, P., Pinkse, P. W. H. & Rempe, G. Dynamics of single-atom motion observed in a high-finesse cavity. *Phys. Rev. Lett.* **82,** 3791–3794 (1999).
5. Rempe, G. One atom in an optical cavity: Spatial resolution beyond the standard diffraction limit. *Appl. Phys. B* **60,** 233–237 (1995).

6. Quadt, R., Collett, M. & Walls, D. F. Measurement of atomic motion in a standing light field by homodyne detection. *Phys. Rev. Lett.* **74,** 351–354 (1995).
7. Mabuchi, H., Turchette, Q. A., Chapman, M. S. & Kimble, H. J. Real-time detection of individual atoms falling through a high-finesse optical cavity. *Opt. Lett.* **21,** 1393–1395 (1996).
8. Münstermann, P., Fischer, T., Pinkse, P. W. H. & Rempe, G. Single slow atoms from an atomic fountain observed in a high-finesse optical cavity. *Opt. Commun.* **159,** 63–67 (1999).
9. Mabuchi, H., Ye, J. & Kimble, H. J. Full observation of single-atom dynamics in cavity QED. *Appl. Phys. B* **68,** 1095–1108 (1999).
10. Hu, Z. & Kimble, H. J. Observation of a single atom in a magneto-optical trap. *Opt. Lett.* **19,** 1888 (1994).
11. Ruschewitz, F., Bettermann, D., Peng, J. L. & Ertmer, W. Statistical investigations on single trapped neutral atoms. *Europhys. Lett.* **34,** 651–656 (1996).
12. Haubrich, D. *et al.* Observation of individual neutral atoms in magnetic and magneto-optical traps. *Europhys. Lett.* **34,** 663–668 (1996).
13. Neuhauser, W., Hohenstatt, M., Toschek, P. E. & Dehmelt, H. Localized visible Ba^+ mono-ion oscillator. *Phys. Rev. A* **22,** 1137–1140 (1980).
14. Wineland, D. J. & Itano, W. M. Spectroscopy of a single Mg^+ ion. *Phys. Lett. A* **82,** 75–78 (1981).
15. Ye, Y., Vernooy, D. W. & Kimble, H. J. Trapping of single atoms in cavity QED. *Phys. Rev. Lett.* **83,** 4987–4990 (1999).
16. Berman, P. R. (ed.) *Cavity Quantum Electrodynamics* (Academic, San Diego, 1994).
17. Horak, P., Hechenblaikner, G., Gheri, K. M., Stecher, H. & Ritsch, H. Cavity-induced atom cooling in the strong coupling regime. *Phys. Rev. Lett.* **79,** 4974–4977 (1997).
18. Hechenblaikner, G., Gangl, M., Horak, P. & Ritsch, H. Cooling an atom in a weakly driven high-Q cavity. *Phys. Rev. A* **58,** 3030–3042 (1998).
19. Carmichael, H. *An Open Systems Approach to Quantum Optics* (Springer, Berlin, 1993).
20. Mølmer, K., Castin, Y. & Dalibard, J. Monte Carlo wave-function method in quantum optics. *J. Opt. Soc. Am. B* **10,** 524–538 (1993).
21. Mancini, S., Vitali, D. & Tombesi, P. Stochastic phase space localization for a single trapped particle. *Phys. Rev. A* (in the press).
22. Cirac, J. I., Zoller, P., Kimble, H. J. & Mabuchi, H. Quantum state transfer and entanglement distribution among distant nodes in a quantum network. *Phys. Rev. Lett.* **78,** 3221–3224 (1997).
23. Law, C. K. & Eberly, J. H. Arbitrary control of a quantum electromagnetic field. *Phys. Rev. Lett.* **76,** 1055–1058 (1996).
24. Law, C. K. & Kimble, H. J. Deterministic generation of a bit-stream of single-photon pulses. *J. Mod. Opt.* **44,** 2067–2074 (1997).
25. Kuhn, A., Hennrich, M., Bondo, T. & Rempe, G. Controlled generation of single photons from a strongly coupled atom-cavity system. *Appl. Phys. B* **69,** 373–377 (1999).

Acknowledgements

We thank P. Münstermann for important contributions to the experiment. The experiments were performed at the University of Konstanz. Funding by the Deutsche Forschungsgemeinschaft, the Optikzentrum Konstanz and the TMR network 'Microlasers and Cavity QED' is gratefully acknowledged.

Correspondence and requests for materials should be addressed to G. R. (e-mail: Gerhard.Rempe@mpq.mpg.de).

An algorithmic benchmark for quantum information processing

E. Knill*, R. Laflamme*, R. Martinez* & C.-H. Tseng†

* *Los Alamos National Laboratory, MS B265, Los Alamos, New Mexico 87545, USA*

† *Department of Nuclear Engineering, MIT, Cambridge, Massachusetts 02139, USA*

Quantum information processing offers potentially great advantages over classical information processing, both for efficient algorithms[1,2] and for secure communication[3,4]. Therefore, it is important to establish that scalable control of a large number of quantum bits (qubits) can be achieved in practice. There are a rapidly growing number of proposed device technologies[5–11] for quantum information processing. Of these technologies, those exploiting nuclear magnetic resonance (NMR) have been the first to demonstrate non-trivial quantum algorithms with small numbers of qubits[12–16]. To compare different physical realizations of quantum information processors, it is necessary to establish benchmark experiments that are independent of the underlying physical system, and that demonstrate reliable and coherent control of a reasonable number of qubits. Here we report an experimental realization of an algorithmic benchmark using an NMR technique that involves coherent manipulation of seven qubits. Moreover, our experimental procedure can be used as a reliable and efficient method for creating a standard pseudopure state, the first step for implementing traditional quantum algorithms in liquid state NMR systems. The benchmark and the techniques can be adapted for use with other proposed quantum devices.

In NMR experiments the qubits are given by coupled spin-half nuclei in a molecule[9,10]. A large number of identical molecules are dissolved in a liquid and used as an ensemble of quantum registers. Control is by radio frequency (r.f.) pulses. The initial state is the thermal state and the readout is an ensemble measurement using standard NMR methods. By preparing pseudopure states, it is possible to benchmark quantum algorithms involving up to about ten qubits to determine how reliable the available control methods are. There have been numerous NMR experiments implementing various quantum algorithms[12–15]. The benchmark proposed and implemented here with seven nuclei requires generating a 'cat state' and then decoding it to the standard initial state. For qubits implemented by spins, the standard initial state has all spins down. The cat state consists of an equal superposition of two states: one with all spins up and the other with all spins down. The cat state is among the most fragile states that are used by quantum computers. A high fidelity realization of our benchmark therefore demonstrates excellent coherent control over the system of qubits.

To simplify the discussion, we use a three-qubit example of the cat-state benchmark. We use deviation density matrices[17] for describing states of the nuclei. This means that states are described by the traceless part of the density matrix up to an overall scale. The thermal equilibrium state of a molecule with one proton (H) and two ^{13}C nuclei (C_1 and C_2) at high field in a liquid is given by $\mu_H\sigma_z^{(H)} + \mu_C\sigma_z^{(C_1)} + \mu_C\sigma_z^{(C_2)}$, with μ_H and μ_C the nuclear magnetic moments. The standard Pauli matrices are used as an operator basis, and superscripts on operators refer to the nucleus the operator acts on. The cat-state benchmark for this system begins by eliminating signal from the carbon nuclei to obtain the initial state $\sigma_z^{(H)}$. Next, a sequence of quantum gates[18] is used to achieve the state $\sigma_y^{(H)}\sigma_y^{(C_1)}\sigma_z^{(C_2)}$ (Fig. 1), which is a sum of several coherences[19]. In particular, it contains the three coherence $|000\rangle\langle 111| + |111\rangle\langle 000|$, which is the deviation density matrix for the cat state $(|000\rangle + |111\rangle)/\sqrt{2}$ (where

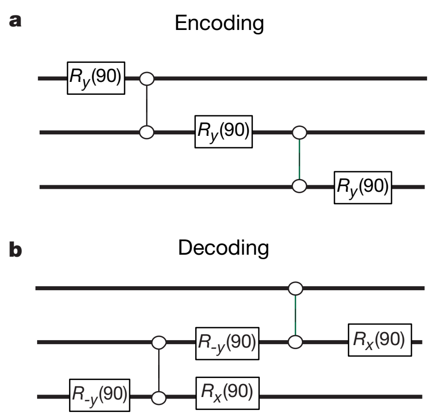

Figure 1 Quantum networks for the cat-state benchmark. **a**, Encoding of the deviation matrix $\sigma_z II$ into $\sigma_y\sigma_y\sigma_x$ by using a cascade of one-qubit rotations ($R_y(90)$) and two-qubit operations (vertical bars) given by *J*-coupling gates. A *J*-coupling gate is given by the unitary operator $e^{-i\sigma_z\sigma_z\pi/4}$. A three coherence $|000\rangle\langle 111| + |111\rangle\langle 000|$ is contained in the output which can be labelled using a magnetic gradient or phase cycling. **b**, Decoding the coherence to a pseudopure state is accomplished by a similar inverse cascade. The output state is $\sigma_x|00\rangle\langle 00|$. Both networks generalize by extending the cascade to more qubits.

